A COMPUTATIONAL STUDY OF BREATH FLOW IN AN ALCOHOL DETECTION SENSOR

by

SHUBHAM NARENDRA RAJESHIRKE

A Thesis submitted to the

School of Graduate Studies

Rutgers, The State University of New Jersey

In partial fulfillment of the requirements

For the degree of

Master of Science

Graduate Program in Mechanical and Aerospace Engineering

Written under the direction of

Dr. Yogesh Jaluria

And approved by

_____

_____

_____

New Brunswick, New Jersey

October 2020

ABSTRACT OF THESIS

A COMPUTATIONAL STUDY OF BREATH FLOW IN AN ALCOHOL DETECTION SENSOR SYSTEM

By SHUBHAM NARENDRA RAJESHIRKE

THESIS DIRECTOR:

Dr. Yogesh Jaluria

Every year many accidents and deaths are caused related to drunk driving in the United States alone. Not only lives are lost but also public and private property destruction is caused. To tackle these ever-occurring problems, the **("DADSS") DRIVER ALCOHOL DETECTION SYSTEM for SAFETY** program was established. This program is responsible to tackle the problems faced due to drunk driving.

This program is directed at developing an alcohol detection system that is capable of detecting whether a driver is impaired by alcohol and take appropriate measures accordingly.

The research focuses on the design of the inlet for the sensor used in alcohol detection in a vehicle and the simulation of breath flow through the inlet designed to retrofit an actual car. This study is carried out to show how the sensor inlet design could be improved if needed. We study what is the effect of variation of flow rate, variation of

inlet area, variation of inlet shape, and change in inclination of the inlet air on the senor inlet. In every variation considered for the study, all the other factors are kept constant.

Results are displayed with the images of flow over and in the sensor inlet. Velocity profiles and velocity contours are shown for all the simulations to grasp a better understanding of how these effects could be potentially used towards the advancement of the research in the future. We can use the conducted research results to further make necessary changes in the design of the sensors if deemed needed.

ACKNOWLEDGEMENT

First and foremost, I would like to thank Dr. Yogesh Jaluria for his technical advice, supervision, and patience throughout my time here at Rutgers. With his invaluable guidance and advice, I was able to complete my Master's thesis successfully.

I am grateful of Dr. Bud Zaouk, CEO and President of KEA technologies for letting me work on this world-changing project, further extending my study on the sensors and writing a thesis on it. I am also grateful to Ryan Stacy for helping me throughout this project and being my link between me and KEA Technologies while I was away at Rutgers. I would also like to thank Cory Novak for helping me understand the chemistry side of the sensor. I would also like to thank the entire staff at KEA Technologies including but not limited to Michael Willis, Philip Bogue, Nick Ouellete and Patric Rooney for helping me whenever needed.

Last, but not least I would like to thank my parents and my sister for being the constant support and trust in me, in this ever-revolving world around me throughout my life. Also, I would like to thank my friends Priyank Ghewari and Omkar Khadilkar for constantly helping me through tough situations and keeping me going. I would also like to thank all my friends for being there who have always helped me go forward in my life.

TABLE OF CONTENTS

LIST OF FIGURES

LIST OF TABLES

CHAPTER 1

INTRODUCTION

1.1 LITERATURE REVIEW

Every year more than 10000 people are killed in drunk driving related accidents in the United States alone and costs exceed $194 billion every year. In order to tackle the problem, the D.A.D.S.S. cooperative research partnership was established. This program is dedicated only for advancing the alcohol detection system for motor vehicles. [1]

This program is researching and developing first of its kind system that, when installed in a vehicle, can detect if the driver is impaired by alcohol. Two technologies are currently being researched under DADSS program [2]

1. Breath based

Figure 1.1 Depiction of Breath based alcohol detection system

The breath-based system uses drivers' normal breath in order to accurately measure the alcohol content when in the driver seat. It is being designed to capture instantaneous breath readings or measurements and successfully tell the difference between the driver and passenger breath.

2. Touch based

The touch-based system uses the driver's touch and uses infrared light to shine through the fingertip and measure the alcohol level in their blood. It is being designed to take multiple readings by the driver's touch to regular vehicle controls such as touch button start or steering wheel or gear shifter for accurate data.

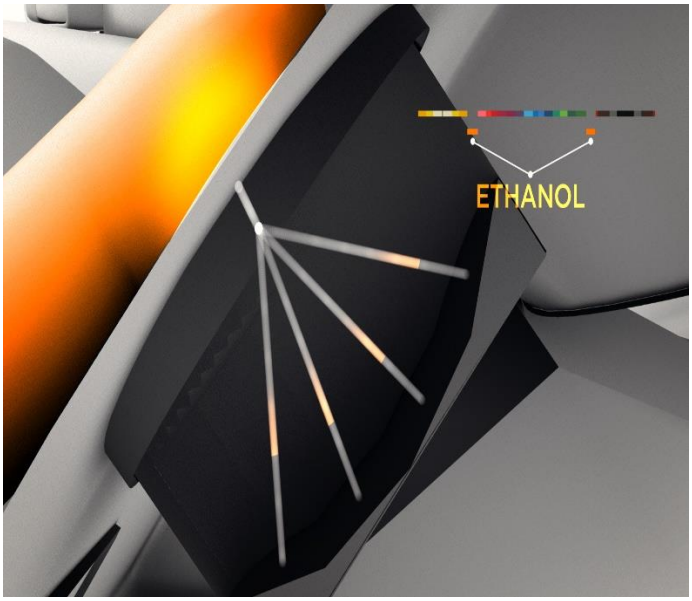

Figure 1.2 Depiction of touch based alcohol detection system

1.2 PREVIOUS WORK

A cooperative agreement was formed in 2008 between ACTS and NHTSA to research and test proof of concept prototypes and determine which technologies could be integrated into existing and new vehicles.[3]

ACTS and NHTSA extended their agreement and the program began a new phase in 2013, which was to reduce the size of the prototypes and establish that the performance specifications are strictly met.[4]

Ever Since 2015 KEA Technologies INC, has been selected as program and technical manager of the cooperative research agreement between NHTSA and ACTS for providing technical guidance and objectively evaluate the technology.[5]

Currently only aftermarket breath testing devices have been used for several decades which can be installed in vehicles and can measure driver's breath alcohol content. These devices are mainly used by drivers who need to provide breath samples before starting their vehicles, primarily convicted of driving while intoxicated. If the breath alcohol concentration is recorded, then the registered vehicle cannot be started. Further investigation into it also indicated that these devices on the vehicles of convicted DWI offenders can reduce the recidivism by about two thirds.[6]

The 2017 paper on Passive in vehicle breath alcohol detection using advanced sensor signal acquisition and fusion, by Jonas L., Bertil H., Amin A., and Hakan P., demonstrates the present status of passive in vehicle driver breath alcohol detection and highlight the necessary conditions for large scale implementation. Their work was built on earlier investigations, in which it has been shown that detection of alcohol vapor in the

proximity of a human subject may be traced to that subject by means of simultaneous recording of carbon dioxide at the same location. They also analyzed video recordings of the subject to determine how body parts including the face are with respect to the breathing behavior and breath detection. Passive in-vehicle driver breath alcohol detection using advanced sensor signal acquisition and fusion.[7]

Today, the use of alcohol detection technology for driver safety is limited to law enforcement testing (during traffic stops/checkpoints or post-accident) or in case of previously convicted DUI offenders through the installation of breath-based vehicle interlocks. The current systems works well for law enforcement purposes but are not suitable for routine use for the public. The main goal of current sensor development is to produce a system that is seamlessly integrated into the vehicle's infrastructure, providing consumers of their alcohol concentration without imposing inconvenience to their daily driving experience.[8]

CHAPTER 2

DESIGN AND SIMULATION OF THE INLET

2.1 Computational Model

The design procedure had a few constraints and requirements. The design was supposed to be completed in a given time frame. As it had to be done in a car after it was off the manufacturing assembly line, everything had to be done manually. It being a prototype, the initial aim was to find a position that will not hinder any other normal vehicle operations while serving the primary purpose of breath detection.

To get the CAD file for the vehicle's dashboard, it had to be manually scanned in 3D. The 3D scanning process was one of the most intriguing process in this experiment. To convert the actual file into a CAD file HandySCAN 700 was used.

Figure 2.1 HandySCAN 3D 700 [9]

The output was a mesh file(.stl), this mesh file was used to recreate a CAD surface with the help of Solidworks. This CAD file was used as a base for modeling the sensor inlet. In 2013, Bertil Hök, Håkan Pettersson, and Jonas Ljungblad wrote a paper on Unobtrusive Breath Alcohol Sensing System [8] in which they discussed about the system and potential locations for the sensors. Taking into consideration various aspects, and previously done work, it was decided that the steering column could be a good position for a sensor placement for this thesis simulation.

The CAD surface was used as a recreation of the steering column on which the sensor inlet was to be retrofitted. The surfacing feature was used to recreate the location on the surface of the vehicle interior. Without hindering the normal operation of the steering column, the sensor was integrated inside of the steering column and the inlet for the breath was placed on top of the steering column facing the driver. [10]

2.2 Actual Model

After the design was ready, HP Jet Fusion 540 was used to 3D print it. With the actual model, stencils also had to be made up to accurately locate and fit the sensor inlet on the steering column with accuracy. The Sensor was installed into a FORD FUSION for testing purposes.

Figure 2.2 HP Jet Fusion 540 [11]

Following are the images of the sensors after they are installed in a vehicle. They are placed to avoid any obstruction with the normal operations of the vehicle and get the readings with ease.

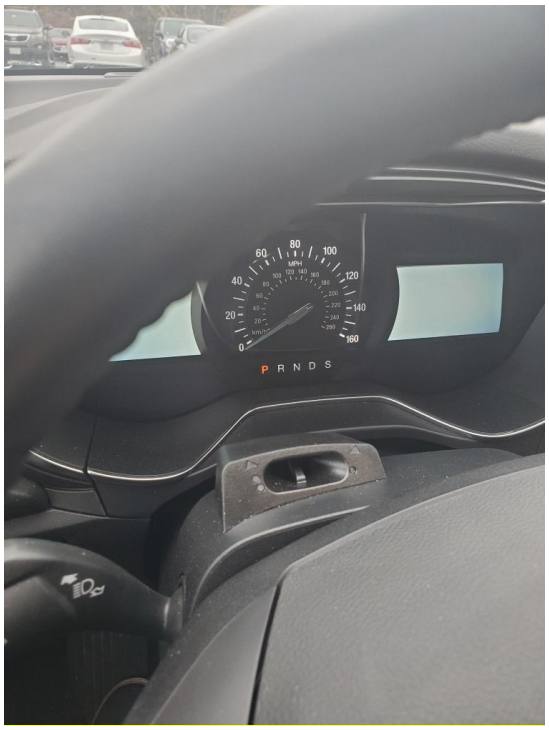

Fig 2.3 Front View

Fig 2.4 Top View

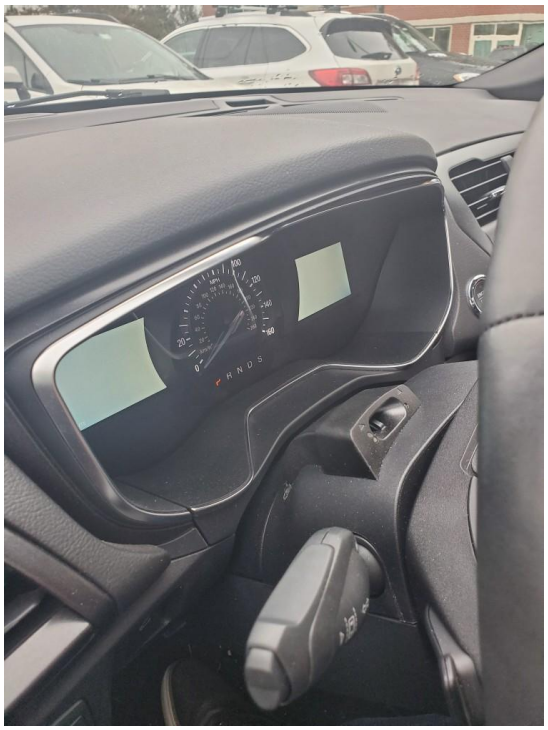

Fig 2.5 Side View

2.3 Simulation Setup

For this study, the main objective of the simulations is to increase the breath capture of a human exhale. Human breath is usually between 5-8 lpm while resting [12]. In order to reduce the time taken by the simulation and fit the simulation within the computational compatibility of the educational version of Ansys, the design was reduced to flow simulation for only a small amount of area over the sensor inlet. The simulation is carried out in four parts:

1. Airflow over the designed sensor inlet and the effects of different airflow rates.
2. The effect of a different shaped inlet area on the air flow through the sensor.
3. How the change in cross-sectional area of inlet affects the air flow through the sensor.
4. The effect of change in the angle of input air flow to the sensor inlet.

The simulation cases are set up as shown in the following tables 2.1, 2.2, 2.3 and 2.4

2.1 Variation of flow rate

Case Number	Area of Inlet X $10^{-4}(m^2)$	Flow Rate (lpm)	Velocity of air (m/s)
1	6.9438	2	0.0490
2	6.9438	2.5	0.0612
3	6.9438	3	0.0734
4	6.9438	3.5	0.0857
5	6.9438	4	0.0979
6	6.9438	4.5	0.1102
7	6.9438	5	0.1224

By considering the flow rate of the air flow inlet varying from 2 to 5 lpm with a constant difference of 0.5 lpm simulations are run. The flow rate is selected from 2 lpm up to 5 lpm in order to replicate the human breath at its lowest point. Although, the working of sensors cannot be discussed in this research, the more volume of breath the sensor inlet can collect the more accurate the detection. As the designed sensor has a fixed opening, the area of the inlet can be set as fixed. So in order to change the flow rate, the velocity of the air can be varied. This was achieved by using conversion of linear velocity to flow rate using the formula:

$$Q = V * A$$

Where,

Q = Flow Rate in m^3/s

V = Average Velocity in m/s

A = Cross-sectional Area in m^2

The conversion factor used for lpm to m^3/s is:

$$1\ lpm = 0.000017\ m^3/s$$

2.2 Variation of Area of Inlet

Case Number	Area of Inlet (x 6.9438 * 10^{-4} m^2)	Flow Rate (lpm)	Velocity of air (m/s)
1	0.5	4	0.0979
2	0.6	4	0.0979
3	0.7	4	0.0979
4	0.8	4	0.0979
5	0.9	4	0.0979

Also, another part of the research was to study how the cross-sectional area of the sensor inlet affects the breath collected by the sensor. In this group of simulations, we will just scale the whole simulation in order to keep all the rest of the factors unchanged to try and obtain accurate results.

2.3 Variation in the shape of the inlet

Case Number	Shape of Inlet	Flow Rate (lpm)	Velocity of air (m/s)
1	Circular	4	0.0979
2	Square	4	0.0979
3	Ellipse	4	0.0979
4	Circular Ellipse	4	0.0979

In 1959 Dean and Hurst [13] analytically studied the motion of fluid in both circular and rectangular curved pipes. They found out that there is more reduction of flow in the square section than in the circular section. Van worked on constricted channel flow in circular and elliptical shapes [14]. Hence, we study the effects of flow rate due to inlet shape with our sensor parameters in order to validate our simulations. For this reason, we use a circular, rectangular, elliptical and circular-elliptical geometry variations and study its effects.

Also, we considered the study of how different shapes of inlet affect can change the amount of breath collected by the sensor. To simplify the experiment basic shapes were used. And which shape helps with the maximum amount of breath captured can be suggested.

In these simulations, the flow rate was kept fixed, and the cross-sectional area was kept constant. The flow rate used was 4 lpm.

Figure 2.6 Circular inlet

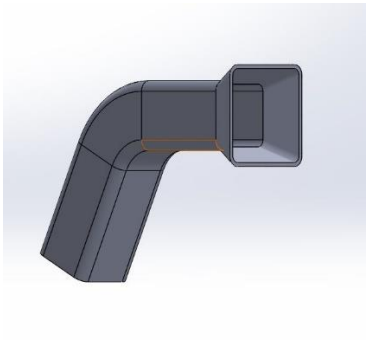

Figure 2.7 Square inlet

Figure 2.8 Elliptical inlet

Figure 2.9 Circular - Elliptical inlet

2.4 Variation in inlet inclination

Case Number	Inlet inclination (degree)	Flow Rate (lpm)	Velocity of air (m/s)
1	10	4	0.0979
2	20	4	0.0979
3	30	4	0.0979
4	40	4	0.0979
5	50	4	0.0979
6	60	4	0.0979

For the last part of the simulation study, the study of how the angle of the input breath(air) given over the sensor inlet with respect to the sensor inlet is studied. All other factors are kept constant.

CHAPTER 3

RESULTS AND DISCUSSION

3.1 Variation in Flow Rate:

As explained in the previous chapter, the computational model for the breath input sensor was validated initially. The first case that was simulated was for 2 lpm flow rate. Other cases consisted of the same constraints and the model, but the flow rate was varied from 2 to 5 lpm varying by 0.5 lpm each. Figures shown below depict how the air flow is over the sensor and in the sensor.

1) For 2 lpm flow rate

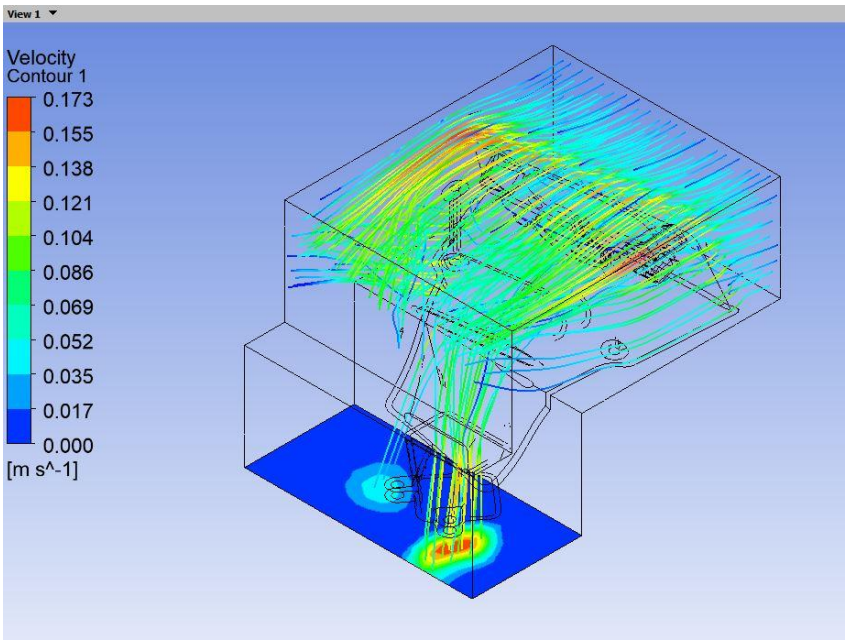

Figure 4.1 Isometric view for 2 lpm flow rate

2) For 2.5 lpm flow rate

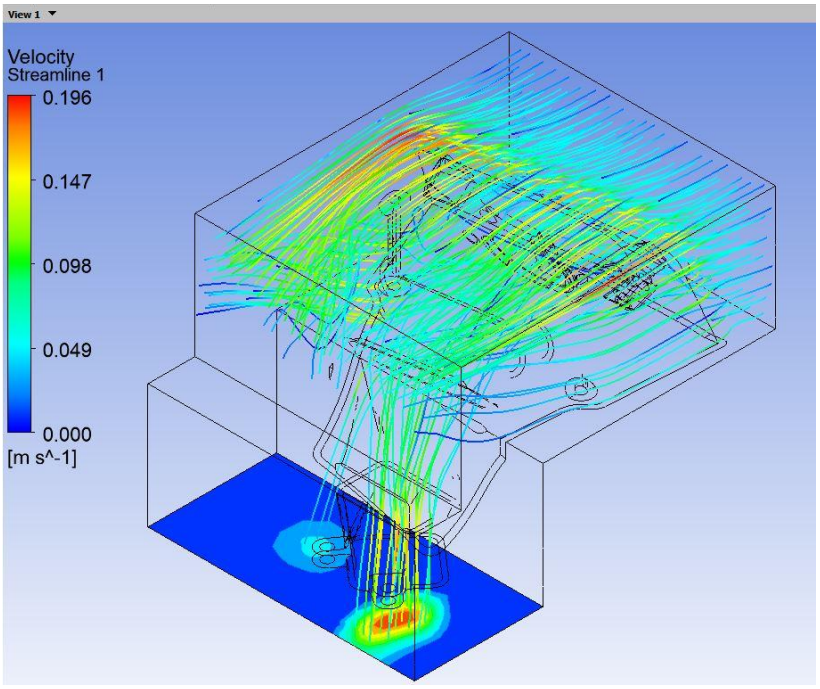

Figure 4.2 Isometric view for 2.5 lpm flow rate

3) For 3 lpm flow rate

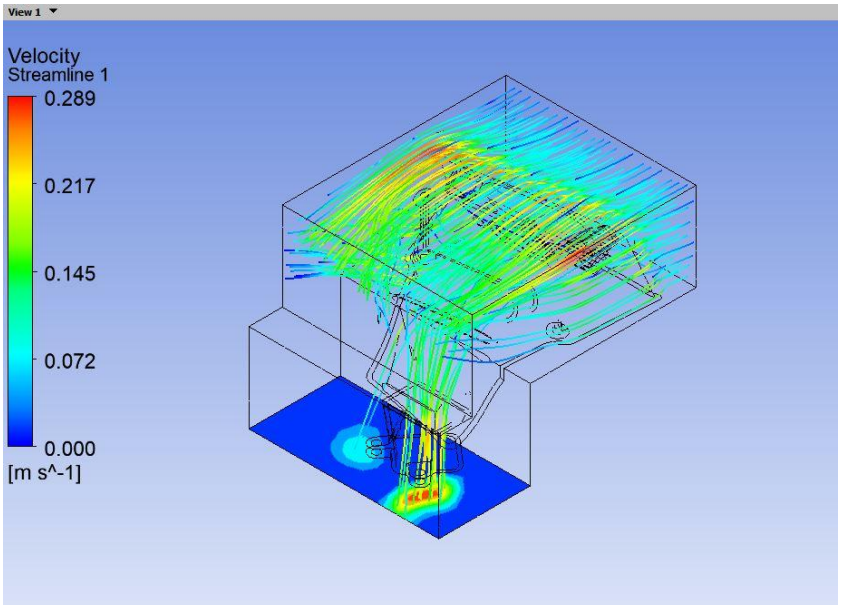

Figure 4.3 Isometric view for 3 lpm flow rate

4) For 3.5 lpm flow rate

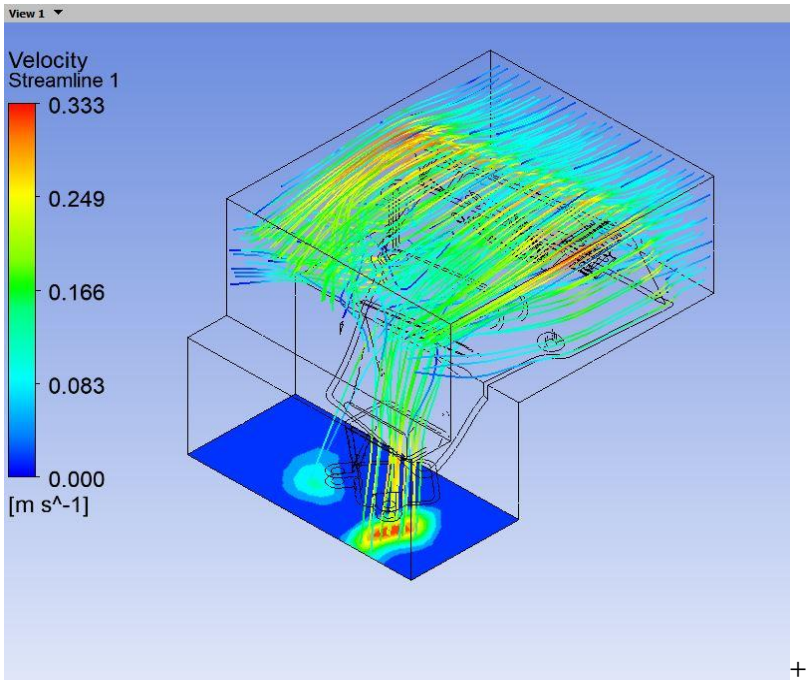

Figure 4.4 Isometric view for 3.5 lpm flow rate

5) For 4 lpm flow rate

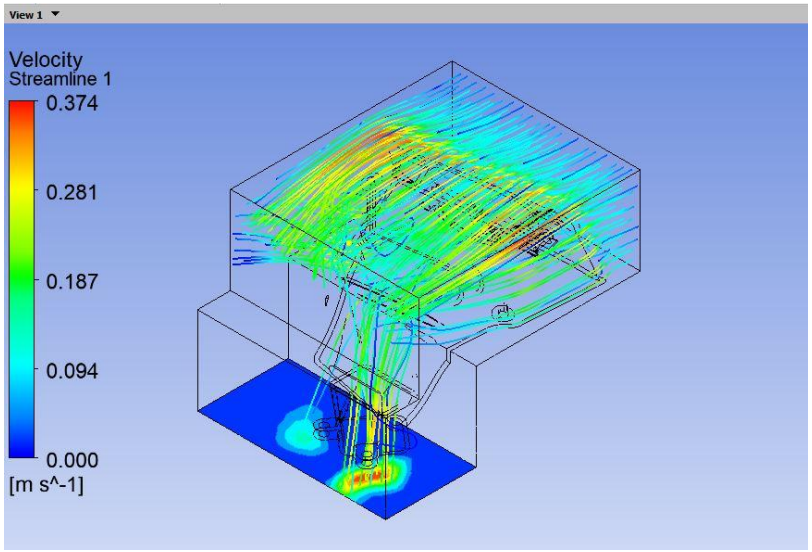

Figure 4.5 Isometric view for 4 lpm flow rate

6) For 4.5 lpm flow rate

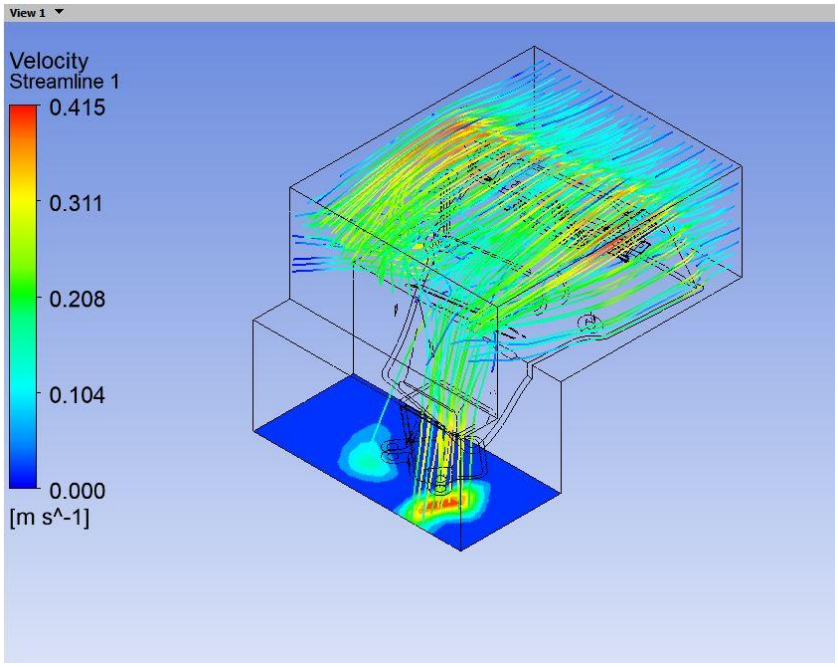

Figure 4.6 Isometric view for 4.5 lpm flow rate

7) For 5 lpm flow rate

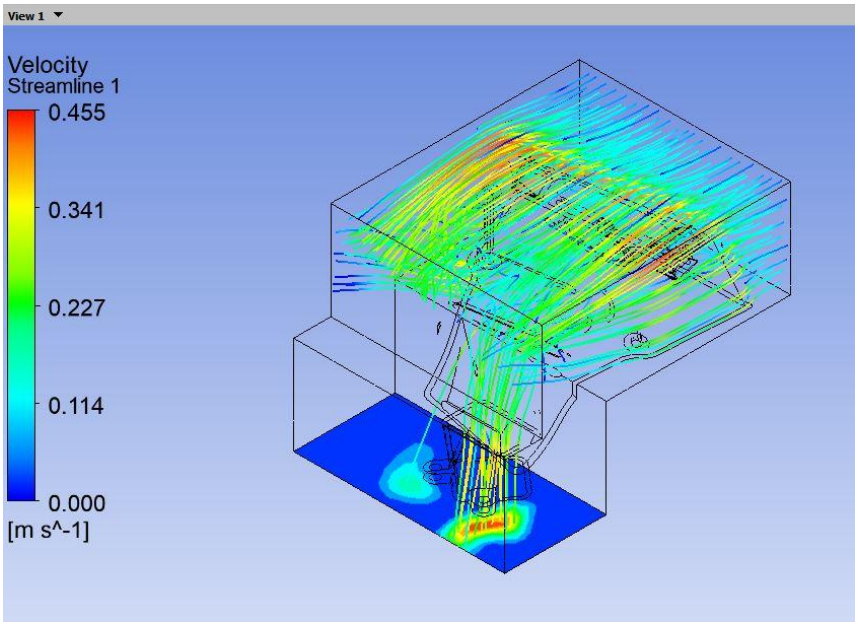

Figure 4.7 Isometric view for 5 lpm flow rate

As seen from the results of the simulation above we can see that the flow pattern within the sensor inlet remains unchanged for the major portion. The changes that occur are in the outlet velocity with respect to the change in input flow rate of the air are observed. As we go on increasing the input flow rates of air the velocity at the outlet and within the sensor goes on increasing. The velocity bar on the left-hand side of the simulation result image above is used for the velocity ranges.

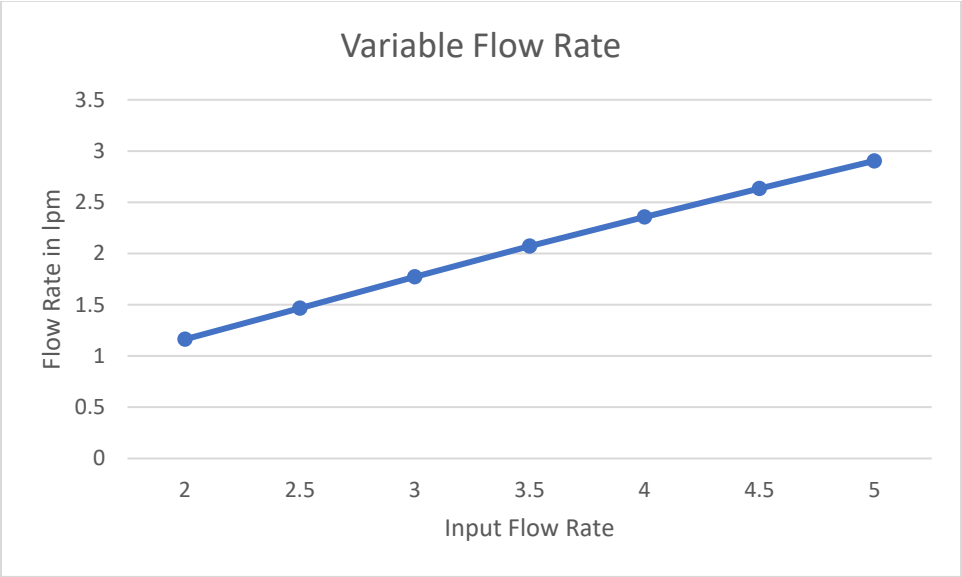

Figure 4.8 Comparison between output flow rate and varied input flow rate

This graph shows the comparison of flow rate provided to the sensor inlet to the output flow rate. As depicted in the graph the output flow rate increases with an increase in input flow rate. This graph can be used to how the sensor behavior should be, it can also be used to determine which flow can be considered to give an accurate and reliable reading. It can be used for fine tuning of the sensor in some special cases which may or may not require more or less amount of breath collection. Hence the curve can be helped to adjust the sensitivity of the sensor.

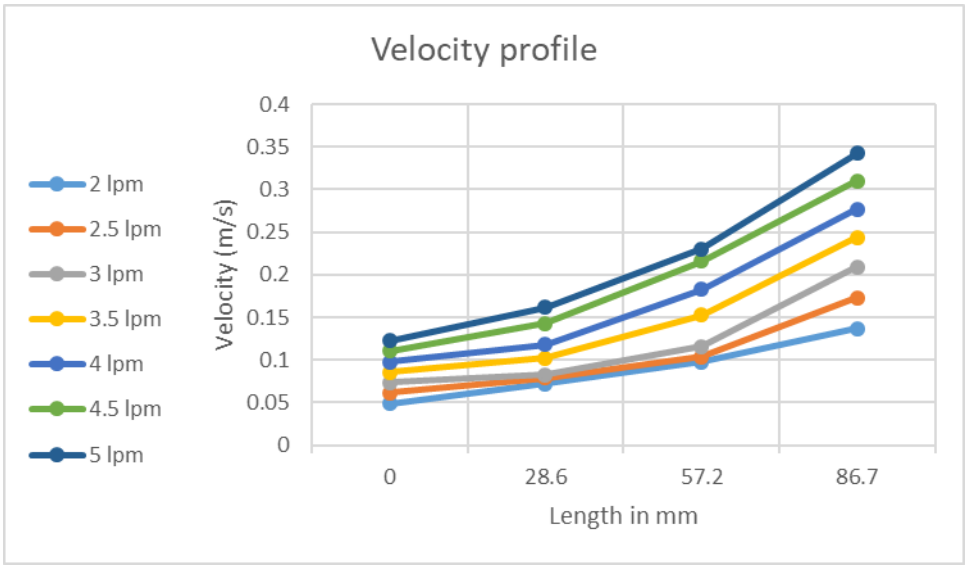

Fig 4.9 Velocity Profile for variable flow rate

The graph shows the comparison between the velocity of the air versus the point at which it was measured. The following graph shows how the velocity profile is inside the sensor inlet body at variable flow rates. The readings are taken at the same points in the inlet body by varying the flow rate, which are, at start of the sensor, at one third length, at two third length and at the end point of the sensor body. The velocity goes on increasing at every measuring point taken. As we can see the behavior of the air flow along the body has similar profiles across all the flow rates that the simulations were run on.

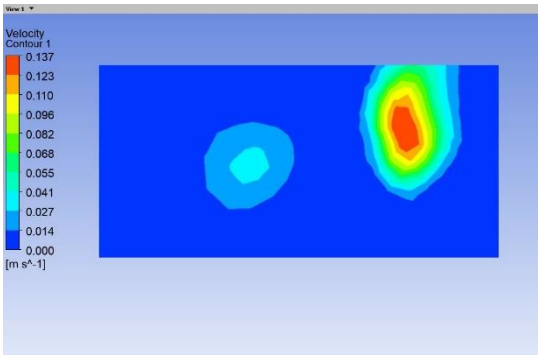

2 lpm

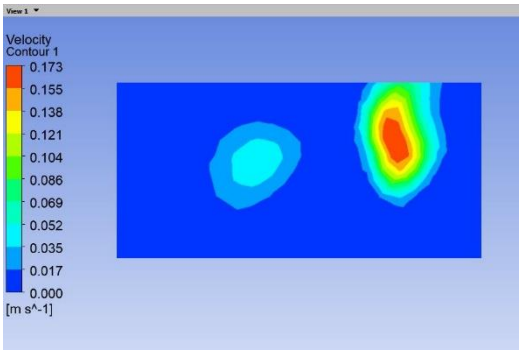

2.5 lpm

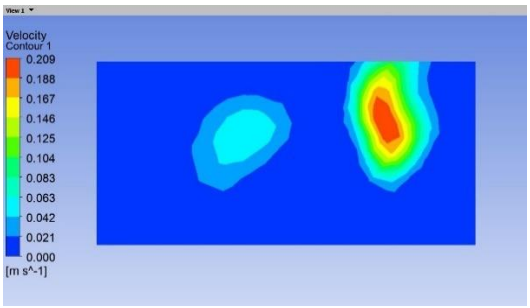

3 lpm

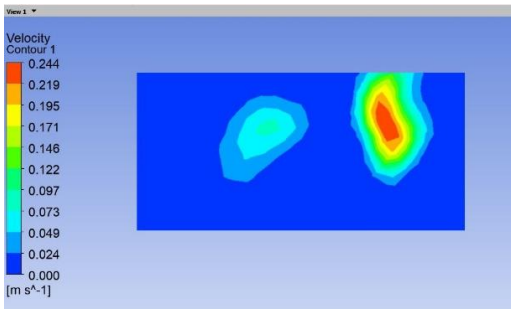

3.5 lpm

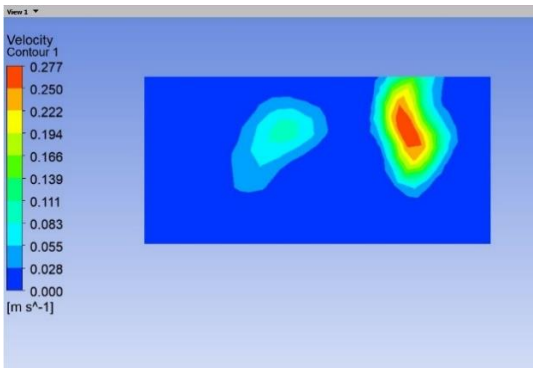

4 lpm

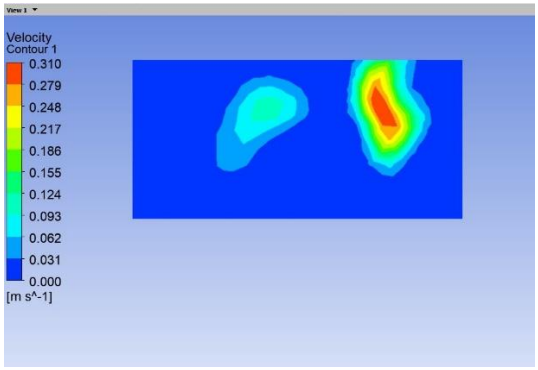

4.5 lpm

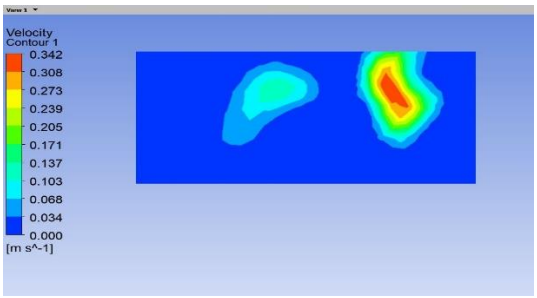

5 lpm

Figure 4.10 Outlet velocity for variable flow rate

The following simulations show the velocity contours at the measuring or processing end of the sensor. We can see the overall profile of the gas remains similar. The velocity is also observed to changes due to the change in the flow rate. The change in the velocity

increases with increase in the flow rate and decreases with the decrease in the flow rate, which is a good thing to observe in this simulation. The majority of the air is seen to be redirected towards the central part of the sensor and only a slight is seen to deviate due to the internal structure or contour of the sensor inlet. The sensor inlet can be redesigned to avoid this bleeding and maximize this flow as well and collect the air sample concentrating around a singular middle area of the sensor.

3.2 Variation of area of inlet

The following simulations depicted below are of varying surface area. The original surface area used in this all other simulations except these are considered as the original/ regular surface are. The cases considered below vary from 0.5 times to 0.9 the original surface area.

1) 0.5 times regular surface area

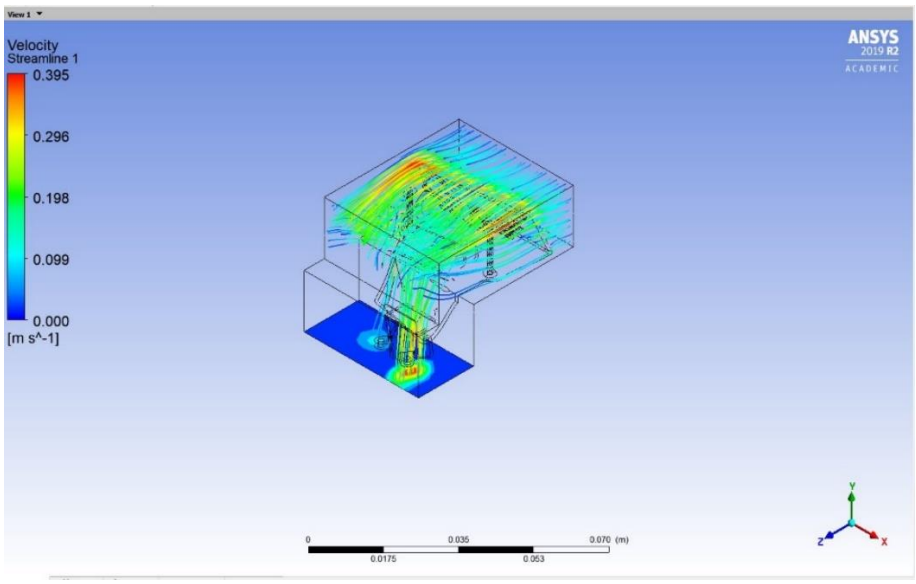

Figure 4.11 Isometric view for 0.5 times initial inlet area

2) 0.6 times initial area inlet

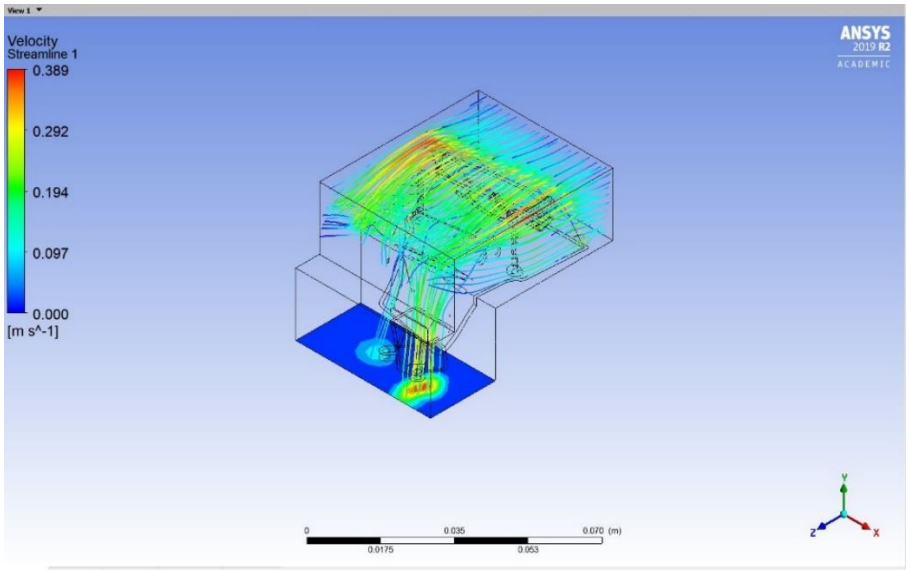

Figure 4.12 Isometric view for 0.6 times initial inlet area

3) 0.7 times initial inlet area

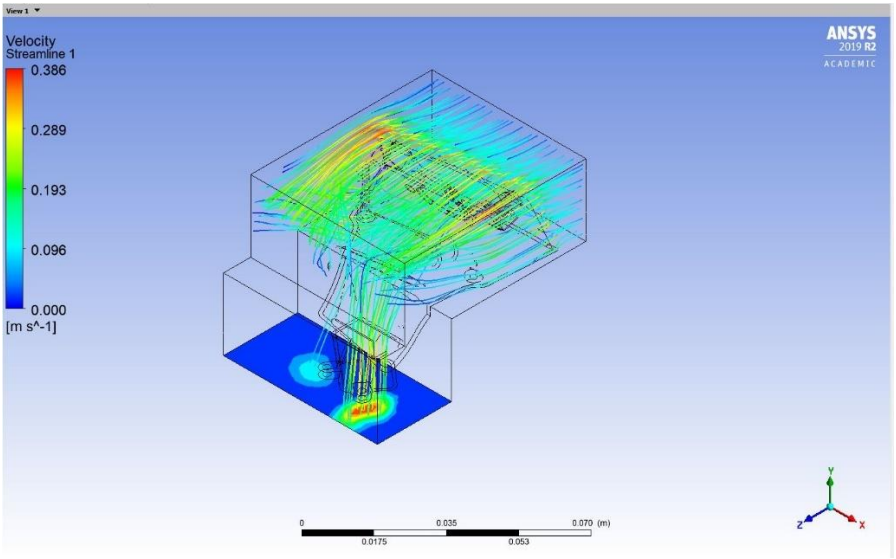

Figure 4.13 Isometric view for 0.7 times initial inlet area

4) 0.8 times initial inlet area

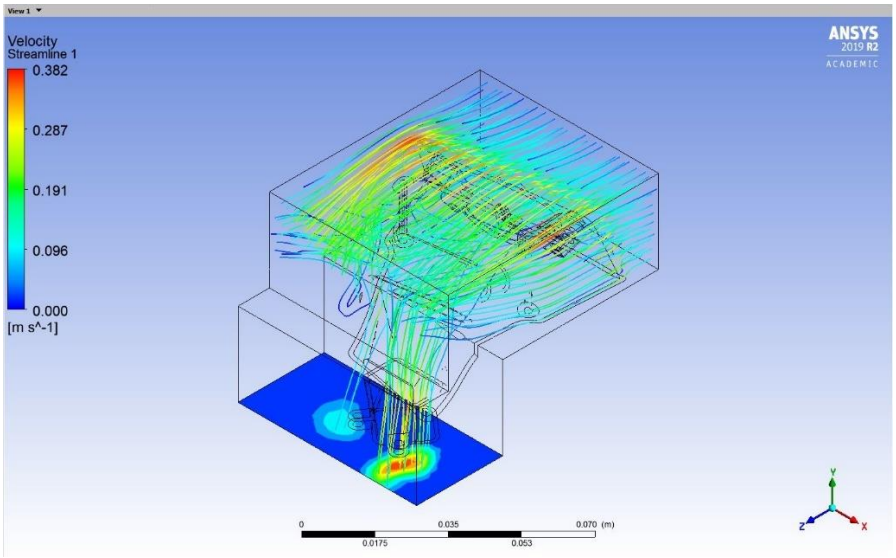

Figure 4.14 Isometric view for 0.8 times initial inlet area

5) 0.9 times initial inlet area

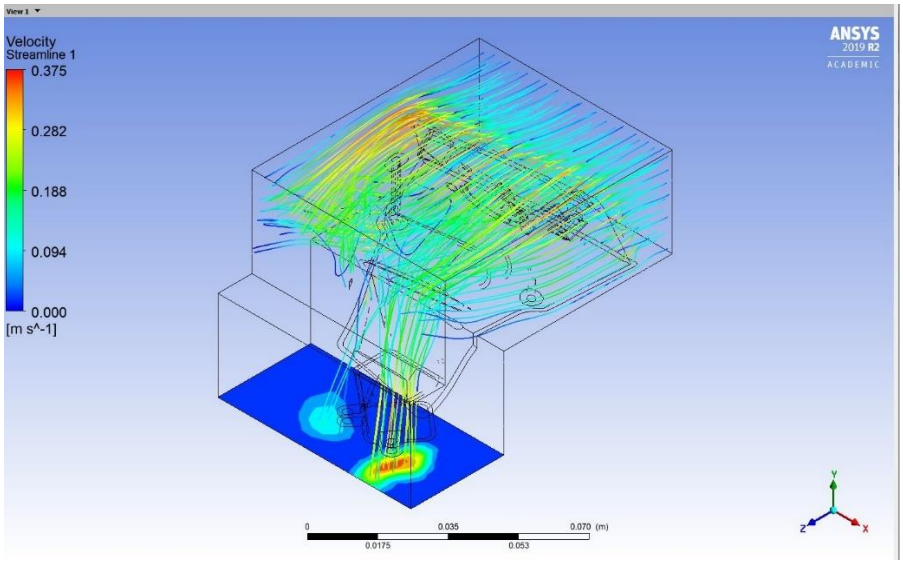

Figure 4.15 Isometric view for 0.9 times initial inlet area

The simulations were run on variation of the initial inlet area. As seen from the results these show that as the size of the inlet area goes on increasing the velocity goes on

decreasing. We know that area and flow rate are directly proportional, and as the area goes on increasing the flow rate should increase as well. Although the velocity goes on decreasing, the increase in area compensates for the decreased velocity observed in the sensor inlet above. This can be seen by the graph plotted below, after the calculation were manually done, after recording the values from the simulations.

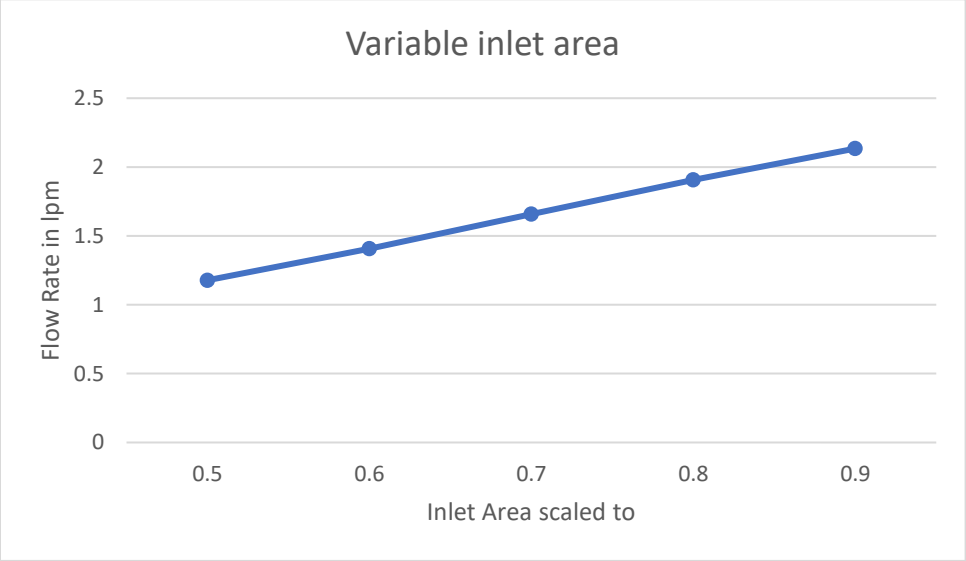

Figure 4.16 Comparison between output flow rate and varied inlet area

The graph shows how the flow rate at the input of the sensor (output of our simulated inlet) changes as compared to area of inlet. The bigger the area is the higher the flow rate is. This can be used to determine the optimum size of the sensor inlet according to the needed accuracy.

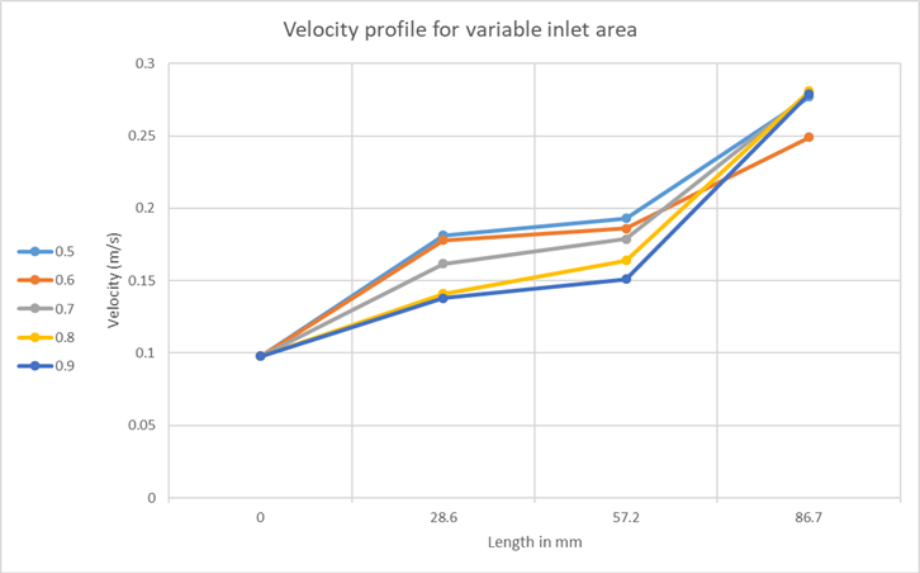

Figure 4.17 Velocity profile for variable inlet area

The graph above depicts the velocity profile of the inlet sensor when the variable inlet area of the collection end is varied. It can be seen that there is a considerable variation in the 0.6 times the surface area of the sensor inlet version. Further investigation will be needed to determine what caused the slight drop in the velocity of the 0.6 times surface area inlet version compared to the others. Also, it can be observed that although the velocity changes over the length of the sensor inlet there is not a considerable change in the behavior except for the 0.6 times the area version.

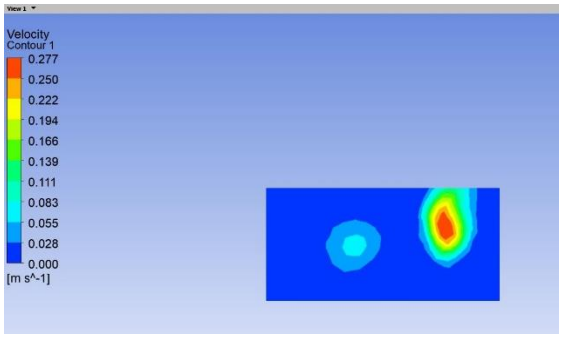

0.5 times

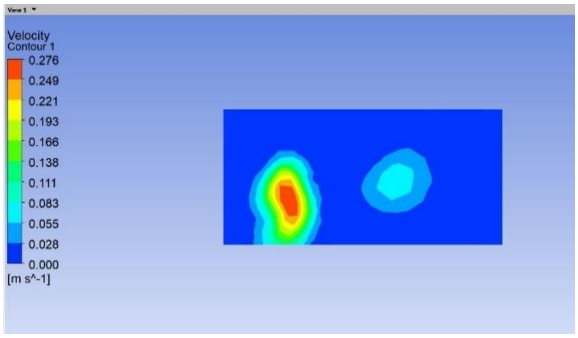

0.6 times

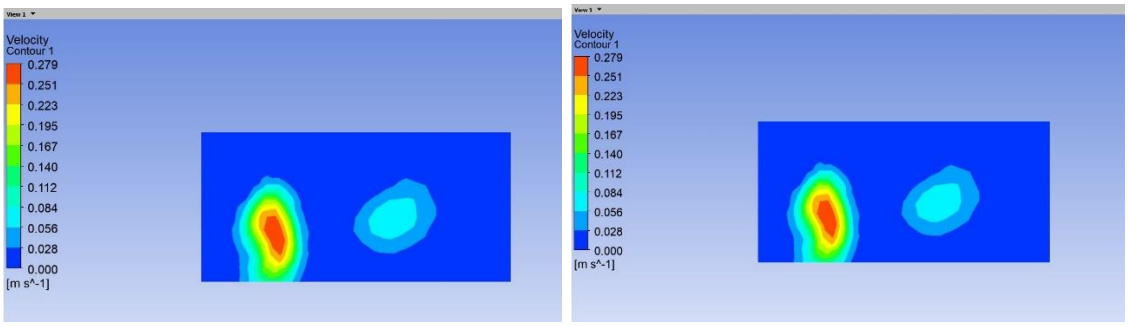

0.7 times 0.8 times

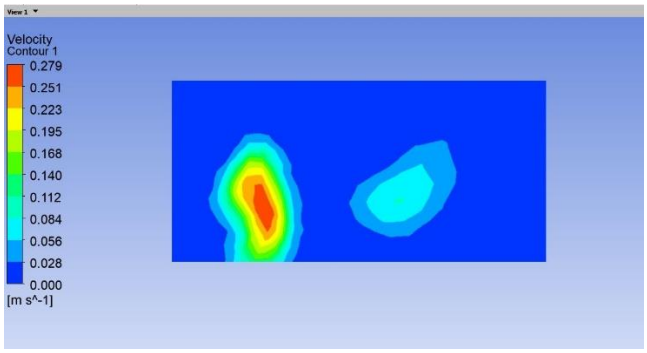

0.9 times

Figure 4.18 Outlet velocity for variable initial inlet areas

As seen above we can say that the velocity profile at the sensor end is similar for variable inlet area. The maximum velocity goes on increasing slightly from 0.5 to 0.7 and is constant for the remaining variations. The velocity is higher at the central area and lower as we go outward. This can be seen as the internal surface of the sensor inlet is designed to avoid blowback towards a specific side other than being centric and inwards. Further investigation is needed to avoid the slight bleeding of the air which can be seen in these images.

3.3 Variation in the shape of the inlet

In these simulations the shape of the inlet is changed in each and every case. Although many more shapes could have been considered, we only considered the basic few shapes for our study. All other factors are kept constant in order to study only the difference between the change in shape by keeping the cross-sectional area constant.

1) For Circular Inlet

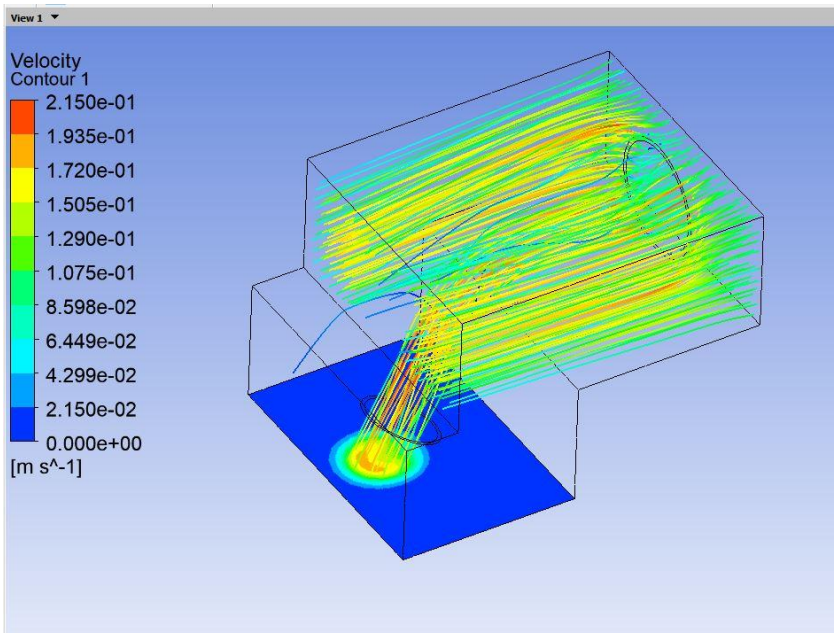

Figure 4.19 Isometric view for circular inlet

2) For Square inlet

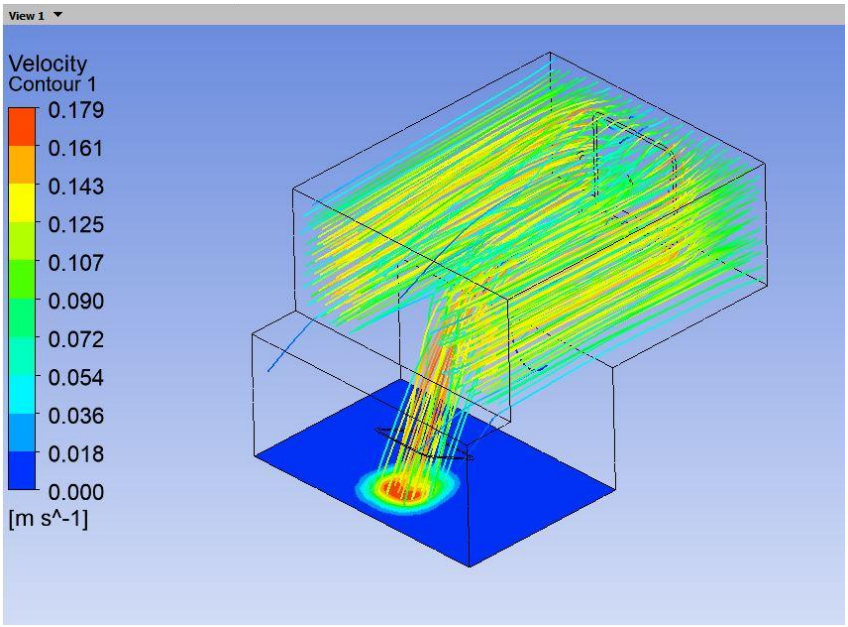

Figure 4.20 Isometric view for square inlet

3) For Ellipse inlet

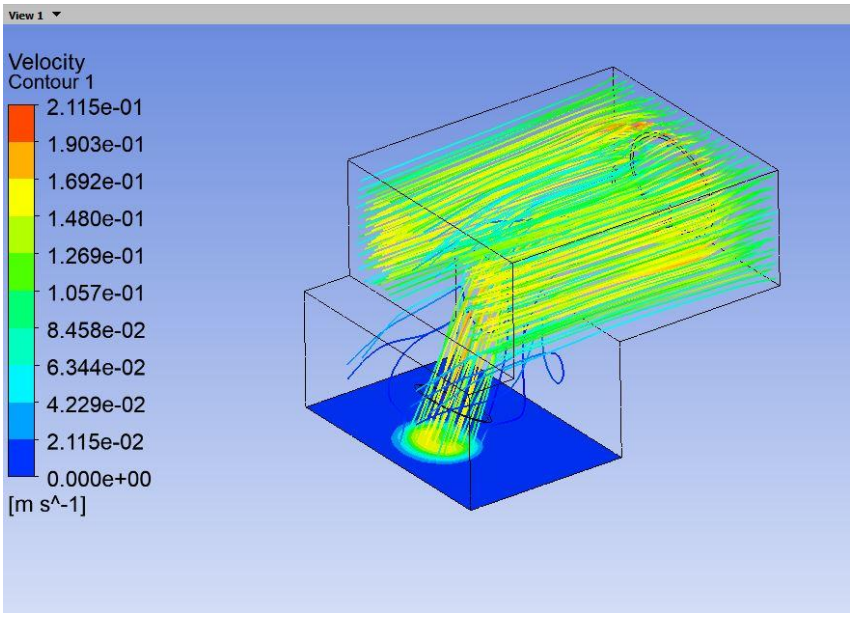

Figure 4.21 Isometric view for elliptical inlet

4) For circular ellipse inlet

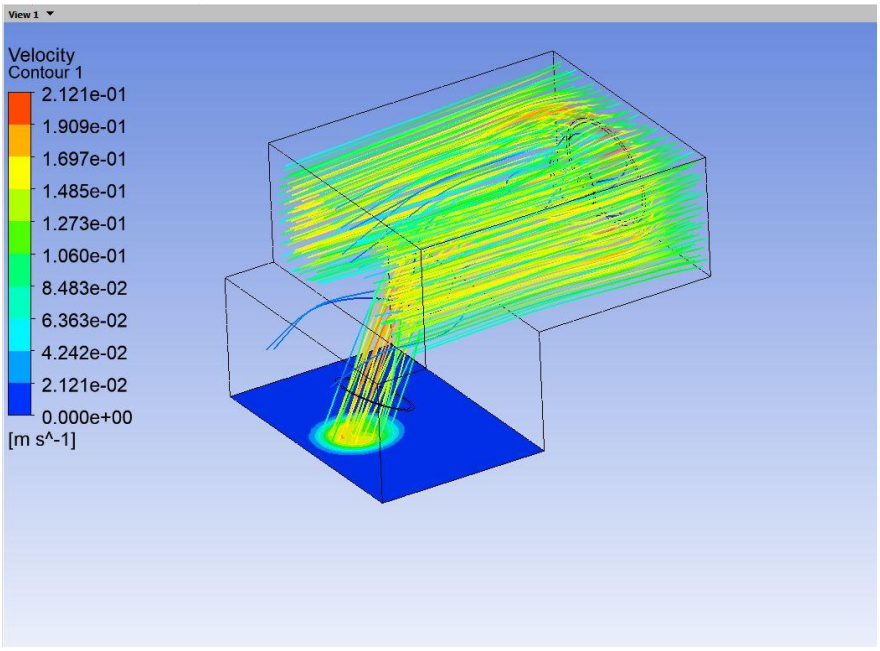

Figure 4.22 Isometric view for circular inner and elliptical outer inlet

We observe from the simulations that the maximum velocities are around 0.215m/s except for the square inlet. The simulations show us the flow pattern of all the different inlet shapes. We see that although the maximim velocities are similar for circular, elliptical and circular-elliptical, there are fewer maximum velocity flow lines in elliptical shape, compared to circular and circular-elliptical.

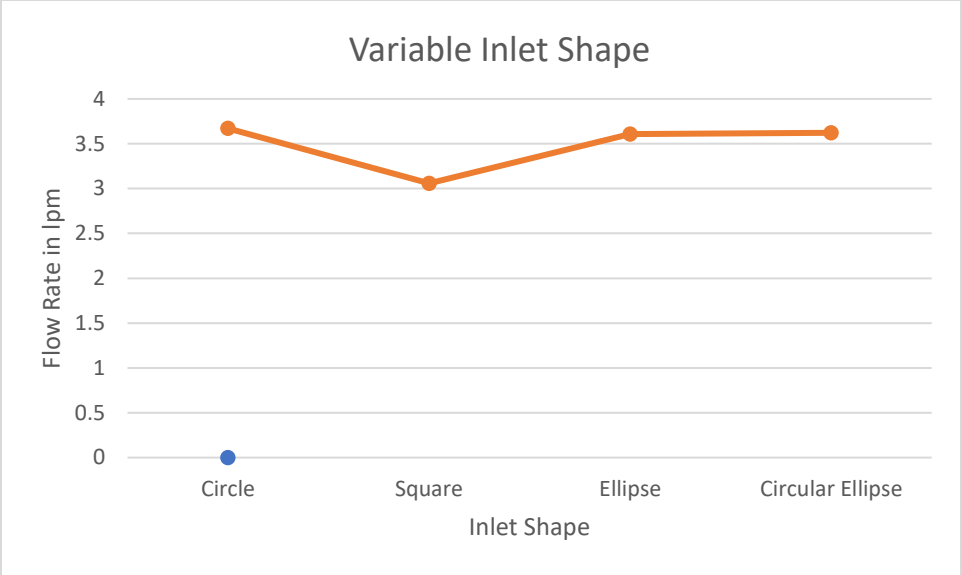

Figure 4.23 Comparison between output flow rate and varied inlet shape

The graph above shows how the amount of air captured by the sensor inlet varies as compared to the shape of the inlet. The circular inlet shows most promising results so as to capture the maximum amount of air that has been blown onto it. Also the circular-elliptical shape of the inlet is used so as to show how the sensor is designed and installed in the car compare with other basic shapes. More shapes can be studied as potential inlet shape but only a collective few were selected for this study. Other shapes could be selected with the acceptable amount of being visually appealing and efficiency tradeoff.

Although the circular shape shows only a slight increase in the air captured as compared to elliptical and circular-elliptical it could be potentially used for the next actual car design so as to increase its efficiency even if it is ever so slightly.

Hatim Azzouz in 2004 [13] mathematically proved the theory that any geometries with their shape more complex than a circular shape will have more resistance to the flow as the contact area with the fluid is more.

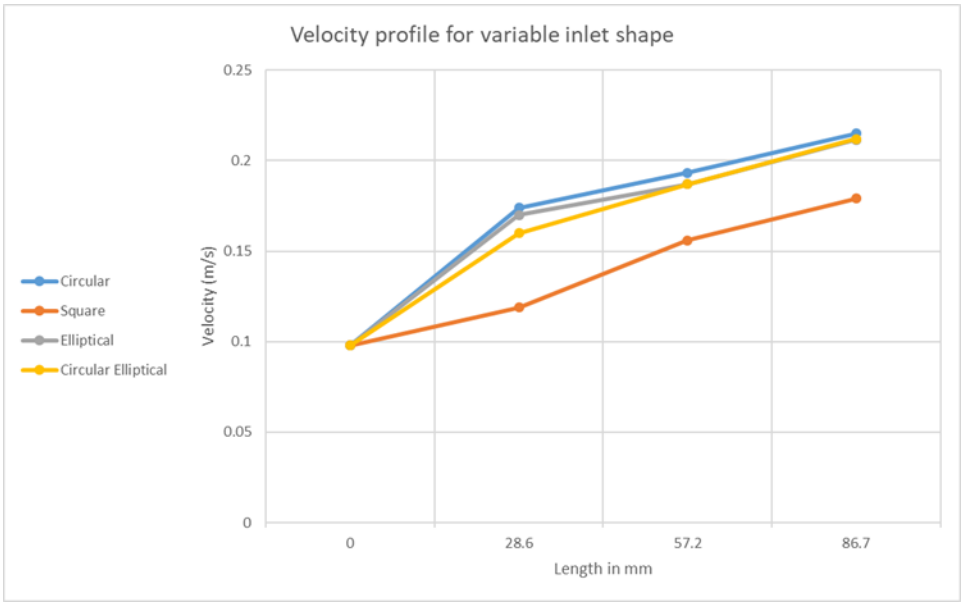

Fig 4.24 Velocity profile for variable inlet shape

Although circular, elliptical and circular-elliptical perform very closely to each other, to maximize the performace circular shaped inlet should be preferred.

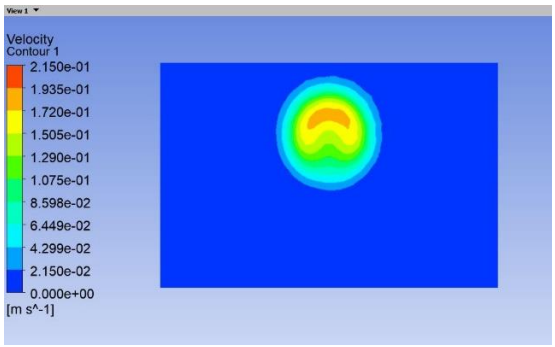

Circular

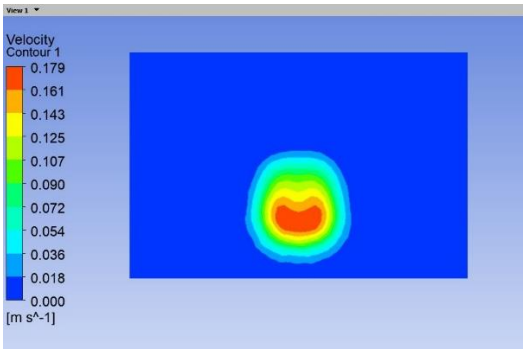

Square

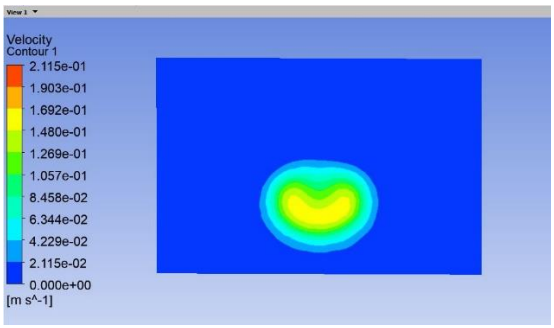

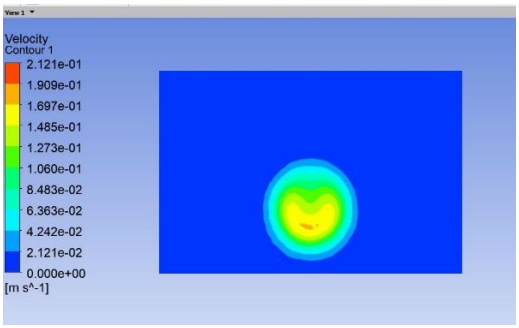

Elliptical Circular inner - Elliptical Outer

Fig 4.25 Outlet velocity contour for variable inlet shape

The velocity contours shown above are comparisons of different shapes and how they affect the velocities or flow rates. As discussed after the isometric views we can see a similar observation here showing lesser higher velocity flow area in elliptical as compared to circular and circular- elliptical. As it can be observed the velocity contours do not differ by much. Even though the velocity contour of the square has more concentration of higher velocities in the center the velocity values recorded are lower in it compared to other shapes.

3.4 Variation in inlet air angle

One of the important factors that would always be a practical issue in this application is the angle at which the breath will be blown on the sensor. This can vary from person to person as the height of the consumer can vary over a broad spectrum. In these simulations we have started with 10° angle with respect to the sensor face. In the rest of the cases the angle of input air has been incremented by 10° each. The effects of this variance are studied below.

1) 10°

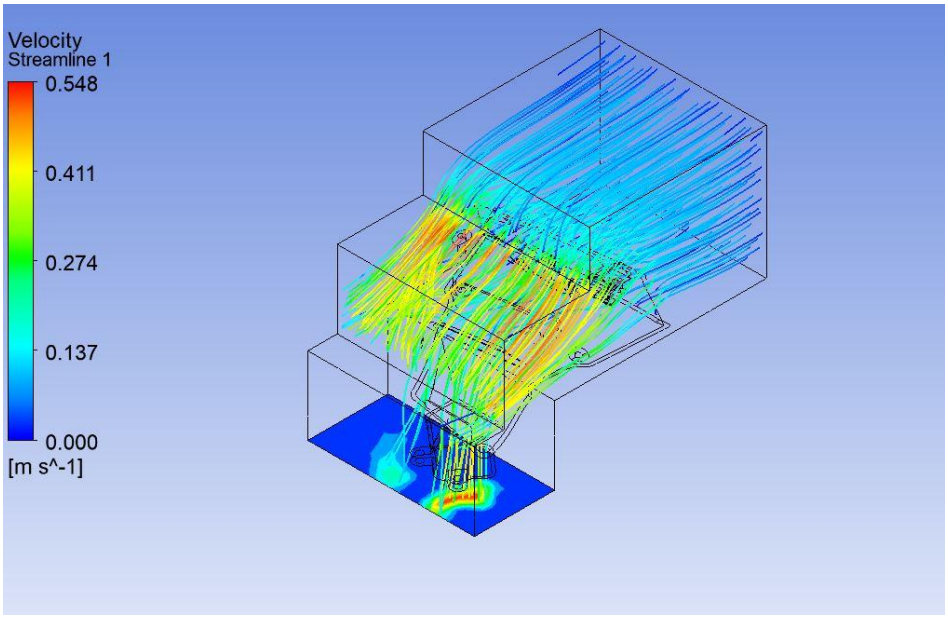

Figure 4.26 Isometric view for 10° inlet angle

2) 20°

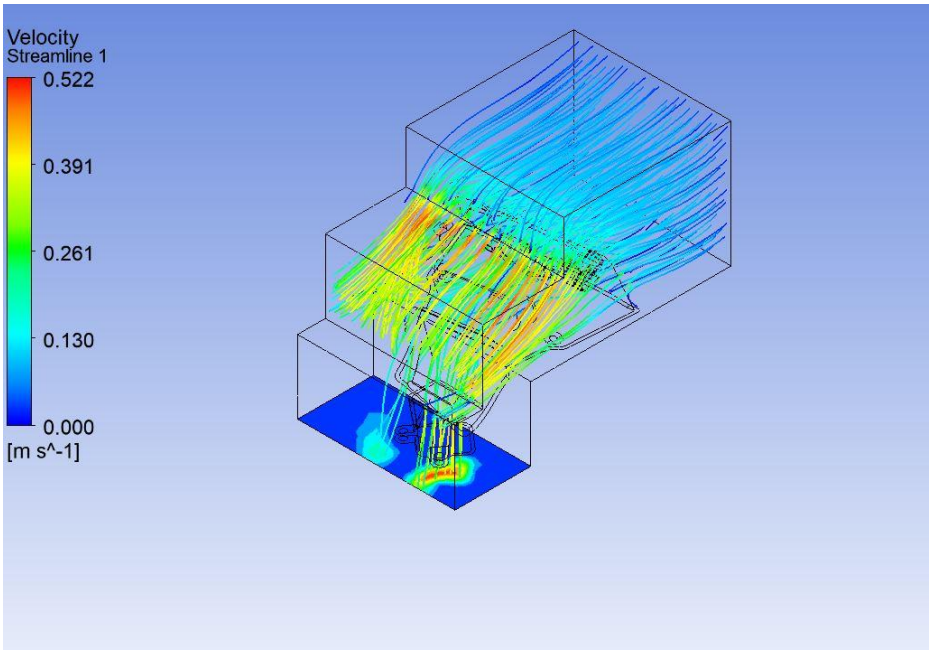

Figure 4.27 Isometric view for 20° inlet angle

3) 30°

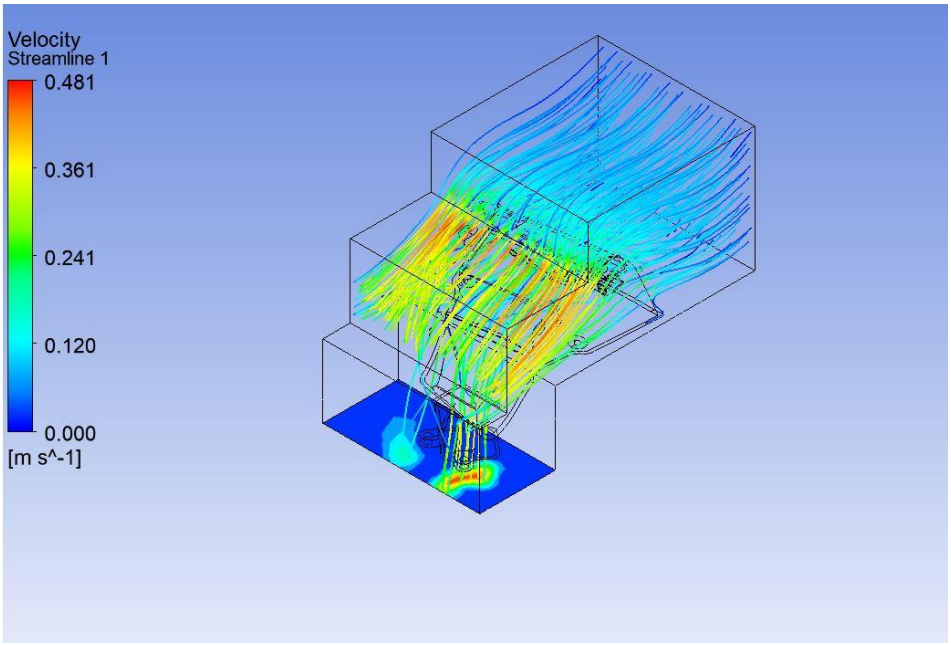

Figure 4.28 Isometric view for 30° inlet angle

4) 40°

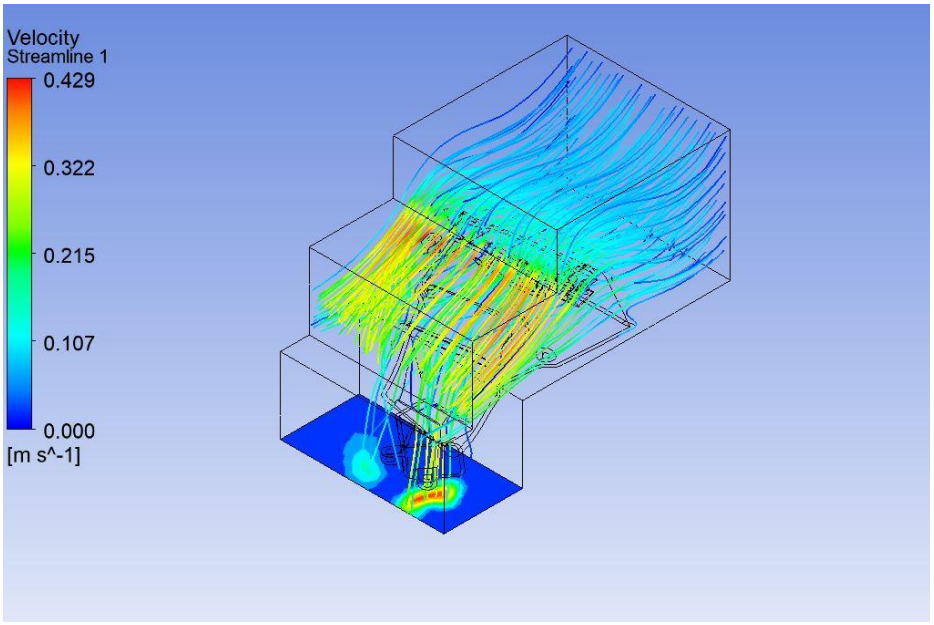

Figure 4.29 Isometric view for 40° inlet angle

5) 50°

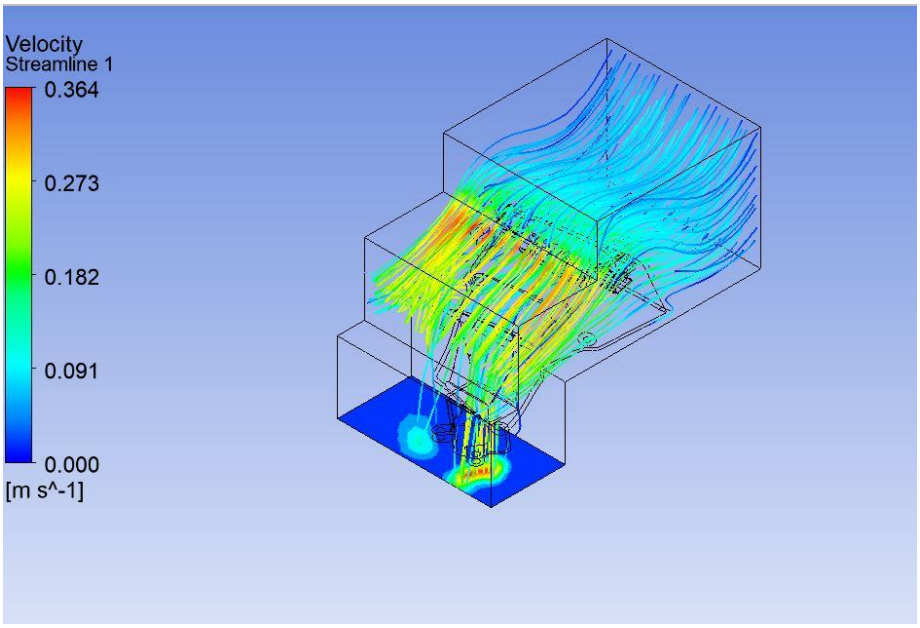

Figure 4.30 Isometric view for 50° inlet angle

6) 60°

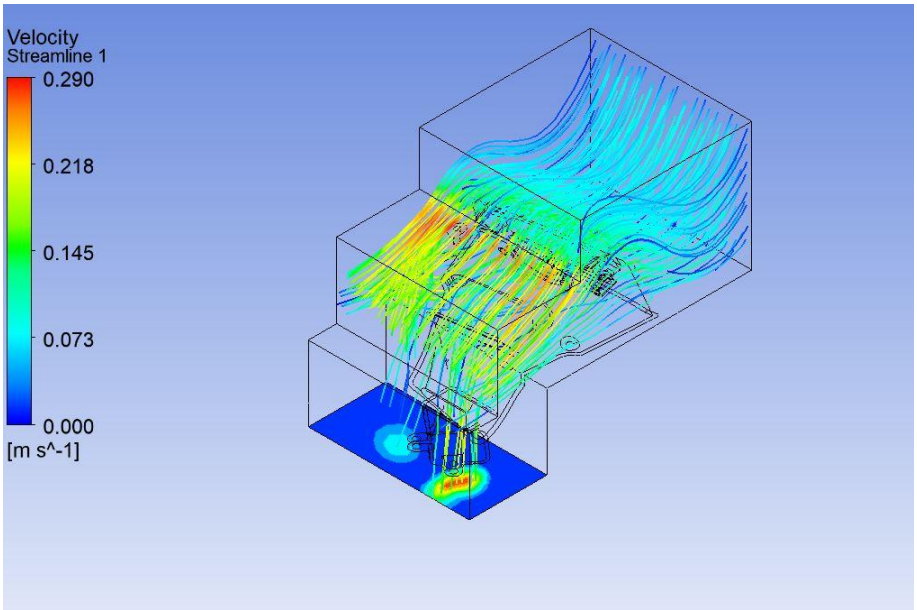

Figure 4.31 Isometric view for 60° inlet angle

These isometric views show the behavior of the sensor inlet with the change in the inlet air flow angle. The views for these simulations differ in the area considered from the previous simulations because the change in angles needed more area to totally cover the inlet surface area of the sensor inlet. But as the rest of the variables are kept constant for this study, it should not be a problem.

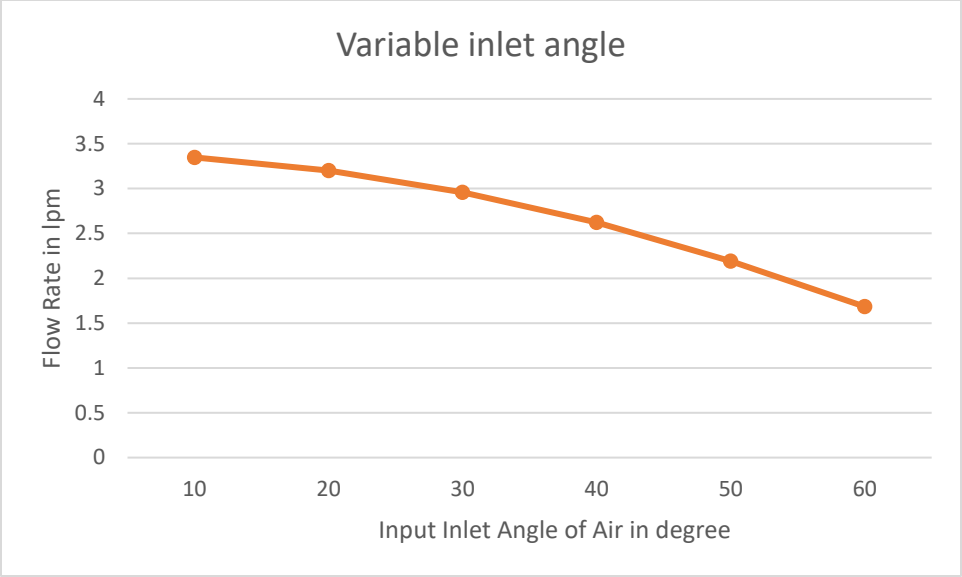

Figure 4.32 Comparison between output flow rate and varied inlet air angle

The following graph is depiction of how the flow rate is affected by the change in the angle of the breath provided. The graph shows the behavior of the sensor inlet with the change in the inlet air flow angle. After plotting, the values obtained through the simulations and hand calculations, it can be said that, the less the angle is in between the sensor inlet and the air direction the greater is the flow rate at the end of the sensor inlet.

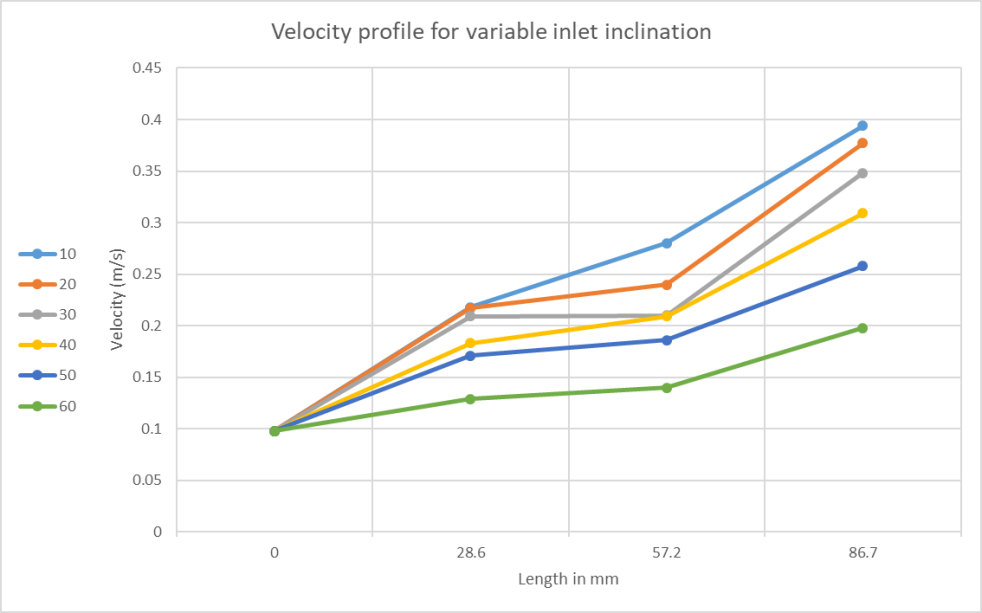

Fig 4.33 Velocity profile for variable inlet angle

The observed velocity profile is the graph for the change of velocity through the sensor inlet by varying the angle of inlet air passed through it. As we can see the velocity goes on gradually decreasing over the length of the sensor. The trend over the length of the sensor is almost similar in all the cases. The velocity goes on increasing as it travels along the length of the sensor inlet. The sensitivity of the sensor can also be controlled with the help of this study.

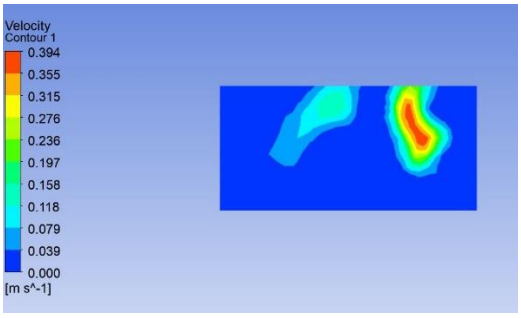

10°

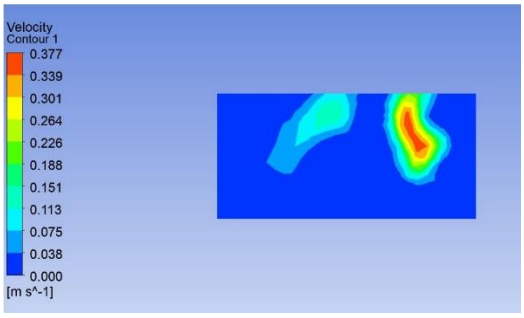

20°

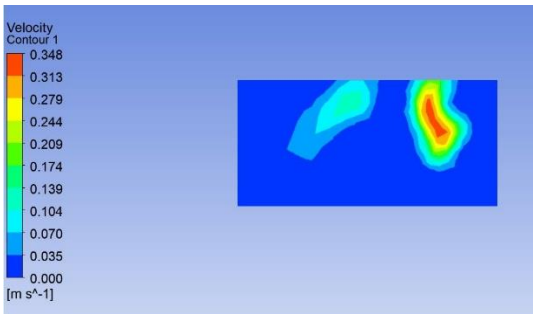

30°

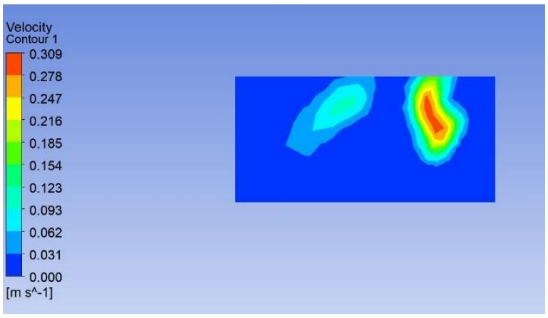

40°

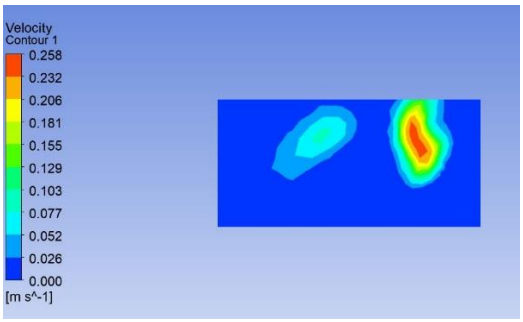

50°

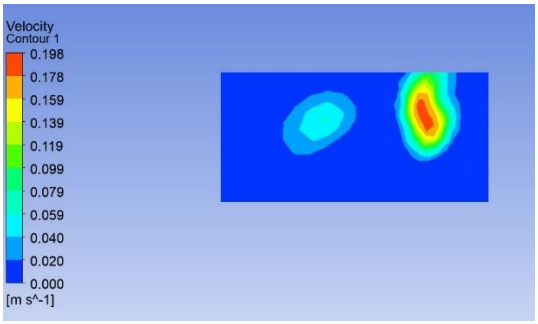

60°

Figure 4.34 Outlet velocity for variable inlet angle

These simulations results shown above shows how changing the inlet angle affects the velocity distribution profile along the width at the end of the sensor inlet. As we can see from the images above we can say that even though the angle of input air to the sensor inlet is varied the velocity distribution profile remains similar. It is higher towards the center and goes on lowering as we move outwards. It can be clearly observed on this angle of the varying simulations that the velocity or the flow rate is higher at lower angles. The stray air that is being shown on the left side of the image can be avoided by investigation and changes in the internal structure of the inlet sensor body.

CHAPTER 4

CONCLUSIONS

The research mainly consisted of the computational simulations of the driver alcohol detection system for safety sensor inlet and how different factors can affect the performance of the sensor inlet. This chapter reviews the conducted research in short and the conclusions for the simulations are as follows:

The variation in flow rate study shows how variation at the inlet (inlet velocity) can affect the flow rate that is read at the sensor end. This factor could be used to help study, limit or change the performance of the sensor depending on the strength of the human breath provided. It can also be possibly used for increasing or reducing the sensitivity of the sensor if need be.

The change in the inlet area of the sensor inlet simulations helped us study the effects of change on the output flow rate at the sensor end. These can be used to determine how the size of the sensor inlet should be inorder to get an optimum or maximum flow rate as required by the sensor to give a reliable and accurate reading. Similarly, this study can also be used to change the sensitivity of the sensor if need be.

From the variation of shapes of the inlet simulations we can say that the circular, elliptical and circular-elliptical shaped inlet can perform much better than the square shaped inlet. Although circular, elliptical and circular-elliptical perform very closely to each other, to maximize the performance circular shaped inlet should be preferred. This study can be used to study or balance the tradeoff between visual representation and performance.

The simulations of the effects of the change in the inlet air angle with respect to the sensor inlet tell us that these results can be potentially used in order to approximately fix the location of the sensor inlet with respect to the driver. These results could also be used to personalize the sensor inlet based on the varied builds of a driver.

CHAPTER 5

FUTURE WORK

There are a lot of other factors other than those of this study which could be used to improve the flow rate capture by the sensor inlet. There will always be tradeoffs between looks, efficiency, cost, etc. The sensor will be needed to be designed with the right balance considering all the factors with the primary aim being, keeping the system accurate and reliable. If the sensitivity, accuracy and reliabi lity ranges are fixed other factors could be potentially varied to make the sensor less and less visible and visually pleasing if need be. Hence we could say that further investigation could be done so as to improve and enhance the sensor inlet.

CHAPTER 6

BIBLIOGRAPHY

[1] Zaouk, A. K., Wills, M., Traube, E., & Stassburger, R. (2015). Driver Alcohol Detection System for Safety (DADSS). A Status Update, 15-0276. doi:www.DADSS.org

[2] Ferguson, S. A. (2012). Alcohol-Impaired Driving in the United States: Contributors to the Problem and Effective Countermeasures. Traffic Injury Prevention, 13(5), 427-441.

[3] https://www.dadss.org/program-overview/

[4] [5] KEA Technologies Inc, website (https://keatechinc.com/)

[6] Ferguson S. A., Eric, T., Zaouk, A. K., Robert, S. (2009). Driver alcohol detection system for safety (dadss) – a non-regulatory approach in the development and deployment of vehicle safety technology to reduce alcohol-impaired driving. á 21st International Technical Conference on the Enhance Safety of Vehicles. Paper Number 09–0464

[7] Ljungblada, J. (2017). High Performance Breath Alcohol Analysis. Mälardalen University Doctoral Dissertation.

[8] Cech, L., Nagolu, M., Rumps, D., Steeg, B. V., Treese, D., Laaksonen, B., Ridder, t. (2015). Introduction of a solid state, non-invasive human touch based alcohol sensor. 24th International Technical Conference on the Enhance Safety of Vehicles. Paper Number 15-0380

[9] Creaform website (https://www.creaform3d.com/en/portable-3d-scanner-handyscan-3d)

[10] Hök, B., Pettersson, H. og Ljungblad, J. (2015). Unobtrusive breath alcohol sensing system. á 24th International Technical Conference on the Enhance Safety of Vehicles. Paper Number 15–0458

[11] https://www.3dnatives.com/en/3D-compare/imprimante/jet-fusion-340

[12] Wikipedia: https://en.wikipedia.org/wiki/Respiratory_minute_volume

[13] W. R. Dean and J. M. Hurst. (1959). Note on the motion of fluid in a curved pipe, Mathematica Volume 6, Issue 1, June 1959, pp. 77-85, https://doi.org/10.1112/S0025579300001947

[14] A. Van Hirtuma, B. W., H. Gao, X.Y. Luo. (2017). Constricted channel flow with different cross-section shapes. European Journal of Mechanics B/Fluids, 63, 1-8. https://doi.org/10.1016/j.euromechflu.2016.12.009.

[15] The dependence of the cross-sectional shape on the hydraulic resistance of microchannels, 2004, Hatim Azzouz

[16] Tang, W. (2006). Application of cfd simulations for short-range atmospheric dispersion over open fields and within arrays of buildings. Á AMS 14th Joint Conference on the Applications of Air Pollution Meteorology with the A&WMA, Atlanta, GA.

17] Andersson, A. K. (2010). Improved breath alcohol analysis with use of carbon dioxide as the tracer gas. Mälardalen University, Mälardalen University, Västerås, Sweden.

[18] Laminar Flow Forced Convection in Ducts by R.K. Shah and A.L. London

[19] S Ferguson, A Zaouk, N Dalal, C Strohl, E Traube, R Strassburger, Driver Alcohol Detection System for Safety(DADSS) – Phase I Prototype Testing and Findings, Proc. 22nd Int. Conf. Enhanced Safety of Vehicles, February
2012, Paper No 11-0230.

[20] A Zaouk, Driver Alcohol Detection System for Safety, Transportation Research Board 90th Annual Meeting, Washington D. C., Jan. 25, 2011.

[21] National Highway Traffic Safety Administration (NHTSA), The Economic and Societal Impact of Motor Vehicle Crashes 2010, Report DOT HS 812 013, May 2014.

[22] A Kaisdotter Andersson, Improved Breath Alcohol Analysis with Use of Carbon Dioxide as the Tracer Gas, Ph.D. Thesis No. 83, Mälardalen University, Västerås-Eskilstuna, Sweden, September 2010.

[23] A B Lumb, Nunn's Applied Respiratory Physiology, 6th Ed., Elsevier, 2005, p. 157-158.

[24] Chou, S.P., Grant, B.F., Dawson, D.A., Stinson, F.S., Saha, T., Pickering, R.P. 2006. Twelvemonth prevalence and changes in driving after drinking. United States, 1991-1992 and 2001-2002. Alcohol Research and Health, 29, 143-151.

[25] Elder, R.W., Shults, R.A., Sleet, D.A., Nichols, J.L., Zaza, S., Thompson, R.S. 2002. Effectiveness of sobriety checkpoints for reducing alcohol-involved crashes. Traffic Injury Prevention, 3, 266-74.

[26] Lund, A.K., McCartt, A.T., Farmer, C.M. 2007. Contribution of Alcohol-Impaired Driving to Motor Vehicle Crash Deaths in 2005.
Proceedings of the T-2007 Meeting of the International Council on Alcohol, Drugs, and Traffic Safety. Seattle, Washington.

[27] Opdam, J.J., Smolders, J.F. 1986 Alveolar sampling and fast kinetics of tetrachloroethene in man. I Alveolar sampling. British Journal of Industrial Medicine, 43, 814-824.

[28] Hök, B., Pettersson, H., Andersson, G. 2006. Contactless measurement of breath alcohol. Proceedings of the Micro Structure Workshop. May, 2006, Västerås, Sweden.

[29] Ferguson, S.A., Zaouk, A., Strohl, C. 2010. Driver Alcohol Detection System for Safety (DADSS). Background and Rationale for Technology Approaches. Society for Automotive Engineers Technical Paper, Paper No. 2010-01-1580, Warrendale, PA: Society of Automotive Engineers.

[30] AW Jones (2010) The relationship between blood alcohol concentration (BAC) and breath alcohol concentration (BrAC): A review of the evidence. (Road Safety Web Publication No. 15). Department of Transport, London.